International Journal of Latest Research in Science and Technology
Volume 4, Issue 1: Page No.42-46, January-February 2015
https://www.mnkpublication.com/journal/ijlrst/index.php
ISSN (Online):2278-5299

LARGE EDDY SIMULATION OF TURBULENT DRAG REDUCTION BY V-SHAPED RIBLETS

[1]Mohsen Jahanmiri , [2]Abdorasoul Bahraini
[1]Faculty of Mechanical & Aerospace Engineering, Shiraz University of Technology, Shiraz, Iran
[2]Faculty of Mechanical & Aerospace Engineering, Shiraz University of Technology, Shiraz, Iran

Abstract*-Turbulent flow over a riblet-covered surface is investigated numerically. The flow field has been simulated using Large Eddy Simulation (LES) technique. Comparison of computed turbulence statistics and mean velocity profile show good agreement with results obtained from Direct Numerical Simulation (DNS). Also, the computed drag on the riblet surfaces is in good agreement with the existing experimental data. It is concluded that Large Eddy Simulation with the proper grid resolution is capable to capture the complex features of the flow like secondary flows over riblets. Moreover, through numerical modeling, the distribution of cross-flow velocity and streamwise vorticity in near-wall fluid field are obtained, which are used to analyze the mechanism of the turbulent drag reduction over riblet surfaces.

Keywords - Drag reduction, Riblet surface, Large eddy simulation, Turbulence structures

I. INTRODUCTION

There are many engineering applications in aeronautics, marine, ground vehicles, and in pipelines that can be greatly benefited from any significant amount of frictional drag reduction. There exists a number of drag reduction methods including microbubbles injection [1], addition of polymers [2], compliant coating [3], hydrophobic surfaces [4] and riblets [5].

Riblets, or wall grooves manufactured in a surface, are attractive drag-reducing devices because of their low production cost and easiness of maintenance. Initial studies on turbulent drag reduction over riblet surfaces were conducted by Walsh [6-9] at NASA Langley Research center.

Walsh investigated several different types of riblet surfaces and found that drag reduction as large as 8% can be obtained provided that s^+ and h^+ are less than 25, where s is the riblet spacing and h is the riblet height. Further studies showed that blade riblets provide the highest level of drag reduction, scalloped riblets provide the second most, and sawtooth riblets provide the least benefit [5]

After Walsh's experiment, many other experiments have been done. Bechert et al. [10, 11] have investigated more thoroughly different configurations of riblets including rectangular, scalloped and shark-skin-shape riblets. They have shown in a fairly comprehensive experimental investigation how drag reduction on ribbed surfaces can be improved.

Lee & lee [12] have used flow visualization techniques to capture cross-sectional images of the streamwise vortex formations above both flat-plate and semi-circular riblet surfaces in drag decreasing and drag increasing conditions. For the case of drag decreasing (s^+=25.2), since large scale longitudinal vortices are larger than the riblet spacing s^+=25.2, most streamwise vortices stay above the riblets and flow above the riblet valley is sufficiently calm. For the case of drag increasing (s^+=40.6) however, the longitudinal vortices are smaller in size than the riblet spacing, most streamwise vortices stay inside the riblet valley, and the high speed on-rush flows frequently penetrate into the riblet valleys [12].

Numerical simulations of turbulent flow have become an important tool for studying the basic physics of turbulence. For predicting the drag reduction with a riblet surface, most researchers use the Direct Numerical Simulation (DNS) method [13-15]. Choi et al. [15] numerically simulated the instantaneous turbulent structures over V-shaped riblets with s^+=20 and s^+=40 using DNS calculation. The drag computed for each riblet configurations were in good agreement with experimental results. Cases with s^+=20 showed 5-6% drag reduction, while cases with s^+=40 showed a drag increase [15]. Although simulation by Reynolds-Averaged Navier–Stokes (RANS) models also have been done by k-ε model [16] and Reynolds Stress Model (RSM) model [17, 18], these models showed less agreement with experimental data. The difficulty in predicting correctly the drag variation when adopting isotropic models like k-ε, one may choose other models as RSM model to obtain the best results [17].

However, the computational cost for DNS is high as it theoretically requires the mesh size to be smaller than the local Kolmogorov scale. In addition, a high Reynolds number leads to a smaller Kolmogorov scale in the flow. Consequently, the grid amount may be beyond the capacity of computers, so the simulation is restricted to a low Reynolds number flow. These limitations have led to low-cost numerical methods such as Large Eddy Simulation (LES), which receives much attention in recent years [19, 20].

The aim of present work is to perform large eddy simulation over V-shaped riblets for analyzing turbulence statistics compared to those above flat plat. We also demonstrate that the LES method has the capability to model characteristics of turbulent flow over riblet surfaces. Results are compared with DNS model. It shows that LES is an efficient method for studying flow characteristics over riblets.

Publication History
Manuscript Received : *21 January 2015*
Manuscript Accepted : *10 February 2015*
Revision Received : *20 February 2015*
Manuscript Published : *28 February 2015*

II. COMPUTATIONAL WORK

Governing equations The governing equations employed for LES are obtained by filtering the time-dependent Navier-Stokes equations. This filtering process effectively filters out turbulent eddies whose scales are smaller than the filter width, which is usually taken to be the mesh size. The resulting equations thus govern the dynamics of large eddies. For incompressible flows, these filtered equations (denoted by the overbar) can be written as:

Continuity:

$$\frac{\partial \rho}{\partial t}+\frac{\partial\left(\rho \bar{u}_i\right)}{\partial x_i}=0 \tag{1}$$

Momentum:

$$\frac{\partial}{\partial t}\left(\rho \bar{u}_i\right)+\frac{\partial}{\partial x_i}\left(\rho \bar{u}_i \bar{u}_j\right)=\frac{\partial}{\partial x_i}\left(\mu \frac{\partial \sigma_{ij}}{\partial x_i}\right)-\frac{\partial \bar{p}}{\partial x_i}-\frac{\partial \tau_{ij}}{\partial x_i} \tag{2}$$

Where σ_{ij} is the stress tensor due to molecular viscosity defined by:

$$\sigma_{ij} \equiv\left[\mu\left(\frac{\partial \bar{u}_i}{\partial x_j}+\frac{\partial \bar{u}_j}{\partial x_i}\right)\right]-\frac{2}{3} \mu \frac{\partial \bar{u}_1}{\partial x_1} \delta_{ij} \tag{3}$$

And τ_{ij} is the subgrid-scale stress (SGS) defined by:

$$\tau_{ij} \equiv \rho \overline{u_i u_j}-\rho \overline{u}_i \overline{u}_j \tag{4}$$

The subgrid-scale stresses resulting from the filtering operation are unknown, and require modeling. The SGS stress tensor τ_{ij} is modeled by an eddy-viscosity concept as in the RANS models:

$$\tau_{ij}-\frac{1}{3} \tau_{kk} \delta_{ij}=-2 \mu_t \bar{S}_{ij} \tag{5}$$

Where μ_t is the subgrid-scale turbulent viscosity. $\bar{S}_{ij}$ is the rate-of-strain tensor for the resolved scale defined by:

$$\bar{S}_{ij}=\frac{1}{2}\left(\frac{\partial \bar{u}_i}{\partial x_j}+\frac{\partial \bar{u}_j}{\partial x_i}\right) \tag{6}$$

To model μ_t, Wall-Adapting Local Eddy-Viscosity (WALE) Method [21] was used. In the WALE model, the eddy viscosity is expressed by:

$$\mu_t=\rho L_s^2 \frac{\left(S_{ij}^d S_{ij}^d\right)^{1/2}}{\left(\bar{S}_{ij} \bar{S}_{ij}\right)^{5/2}+\left(S_{ij}^d S_{ij}^d\right)^{5/4}} \tag{7}$$

Where L_s and S_{ij}^d in the WALE model are defined, respectively, as

$$L_s=\min\left(\kappa d, C_w V^{1/3}\right) \tag{8}$$

$$\mu_t=\rho L_s^2 \frac{\left(S_{ij}^d S_{ij}^d\right)^{1/2}}{\left(\bar{S}_{ij} \bar{S}_{ij}\right)^{5/2}+\left(S_{ij}^d S_{ij}^d\right)^{5/4}} \tag{9}$$

Where κ is the von Karman constant, d is the distance to the closest wall, C_w is the WALE constant, and V is the volume of the computational cell.

Numerical scheme and solution convergence: The flow geometry and coordinate system are shown in Fig. 1. Numerical modeling is done with exact geometries used by Choi et al [15]. Computational geometry consists of a channel whose top wall is a flat wall and bottom wall is covered with riblets. Riblets have triangular cross-section with the riblet ridge angle $\alpha=60°$.

Fully developed turbulent flow over riblets is homogeneous in the streamwise (x) direction, and periodic boundary conditions are used in the streamwise (x) and spanwise (z) directions. The no-slip condition is applied at both walls. The streamwise and spanwise computational periods are $\pi\delta$ and $0.289\pi\delta$, respectively, where δ is half of the distance between the midpoint of tip and valley on a riblet wall and a upper flat wall .Thus it corresponds to the half-width of the plane channel with the same cross-sectional area.

In the simulation performed herein, Reynolds number based on δ and bulk velocity is 2831. This Reynolds number corresponds to $\mathrm{Re}_\tau=\frac{\delta u_\tau}{\nu}=180$ based on a friction velocity $u_\tau=\left(\tau_w/\rho\right)^{0.5}$ which would develop in a plane channel flow with the same bulk Reynolds number

Non-uniform structured grid is used in each direction to discretize the governing equations. Grid independence is studied by changing the number of grids in three dimensions and finally three different grid resolutions are generated. A detailed description of these grids is shown in Table 1. Cross-flow plane of computational grid (case B) is shown in Fig. 2. As it is shown, the grid points are clustered near riblet tips, where the velocity gradients are large.

Computations are initialized by first, obtaining the turbulent solution using k-ω model [22], and then adding synthetic turbulence fluctuations to the solution. Starting from these initial velocity fields, the governing equations were integrated forward in time until the numerical solutions reached statistically steady states. When the statistically-steady state is achieved, then which the statistics is gathered for an additional time of $\Delta t^+=\frac{t u_\tau^2}{\nu}=4000$.

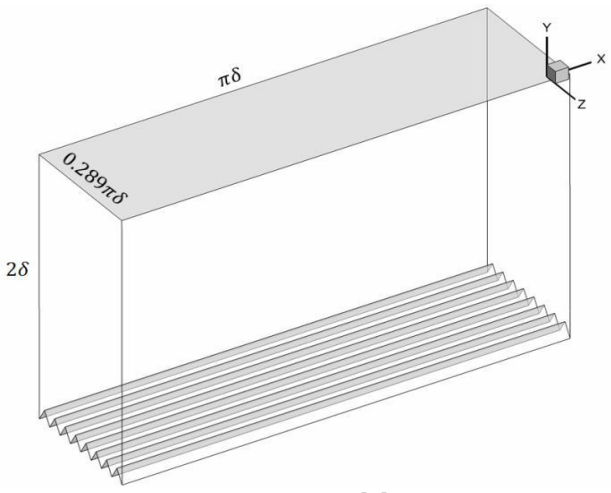

Fig. 1 Computational domain

TABLE 1. GRID PARAMETERS USED FOR GRID INDEPENDENCE STUDY. THE SUPERSCRIPT + INDICATES A NON-DIMENSIOANL QUANTITY SCALED BY THE WALL VARIABLES; FOR EXAMPLE

$$\Delta x^+ = \frac{\Delta x u_\tau}{\nu}$$

Grid type	Grid size	Δx^+	Δy^+	Δz^+
A	16×48×64	35	0.64~29.98	2.56
B	32×64×128	17.5	0.64~19.44	1.28
C	32×96×128	17.5	0.64~12.28	1.28

III. RESULTS AND DISCUSSION

Drag reduction Table 2 shows the drag increase or decrease for each riblet configuration. Also, time history of drag coefficient at both flat and riblet walls for grid B is shown in Fig. 3. The instantaneous plane-averaged drag coefficient is defined on flat (C_{df}) and riblet surfaces (C_{dr}) as:

$$D_f = \mu \int_{A_f} \frac{\partial u}{\partial n} dA_f = C_{df}\left(0.5\rho U_m^2 A_f\right) \quad (10)$$

$$D_r = \mu \int_{A_r} \frac{\partial u}{\partial n} dA_r = C_{dr}\left(0.5\rho U_m^2 A_f\right) \quad (11)$$

Where A_f and A_r are surfaces of the flat wall and riblet wall, respectively. The time-averaged Drag coefficient histories, i.e. $\frac{1}{t}\int_0^t C_{df}(\tau)d\tau$ and $\frac{1}{t}\int_0^t C_{dr}(\tau)d\tau$, are also shown in Fig. 3. Fig. 3 shows that instantaneous drag coefficient at the riblet surface for the most of the time is smaller than the drag at the flat surface, resulting time-averaged values to 7.63×10^{-3} and 8.23×10^{-3}, respectively as reported in Table 2. Grid types B and C show a good drag decrease compared with DNS data (about 6%) [15], but grid A shows drag increase. Because of slight changes in drag reduction from grid B to C, following results are based on grid B. Also comparison of drag reduction between the present work and experimental data (about 4% [7]) shows a rather good agreement.

Turbulence statistics: Fig.s 4-7 show turbulence statistics profiles at various spanwise locations. Flow variables on the side of the channel with the riblets (lower wall) and flat plate (upper wall) are averaged in x, t, and the same spanwise locations over different riblets. Results are presented in global coordinates. Fig. 4 shows mean velocity profile compared with DNS results [15]. In Fig.s 5-7, root-mean-square of velocity fluctuations in streamwise, normal and spanwise direction are presented. Velocity fluctuations are normalized by the centerline velocity U_c, and lengths are normalized by the channel half-width. As it is clear from the figures, the mean velocity profile is overestimated at core of channel. Also, normal velocity fluctuation is underpredicted. These trends have also been observed in other LES works [19]. However, the performed simulations through the LES method along with the WALE model demonstrate an acceptable agreement with the DNS results especially with streamwise and spanwise velocity flactuations. So, large eddy simulation with WALE subgrid-scale model is capable to compute turbulence statistics.

It is interesting to note turbulent intensities for all three velocity components are reduced above the riblet surface compared to the same nondimensional distance from the wall in a flat plate, although reduction in spanwise and normal direction is larger. Also mean velocity profile over riblets is greater than over flat plate, which is consistent with DNS of choi et al. [15].

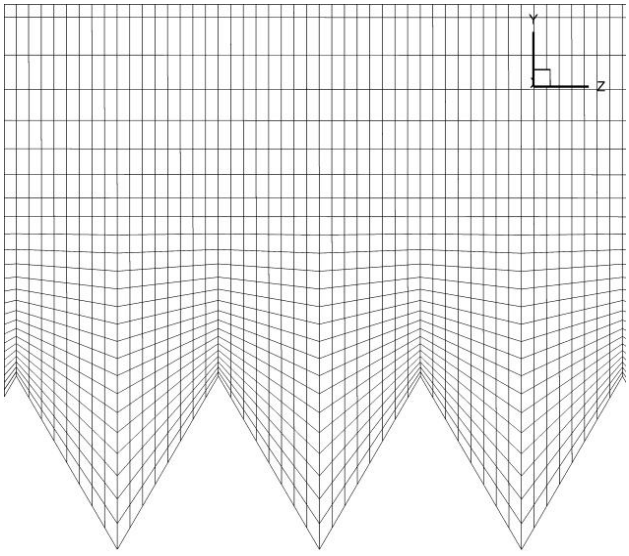

Fig. 2 Computational mesh near riblets for the case B(y-z view)

TABLE 1.DRAG VARIATION FOR EACH GRID TYPE

Grid type	Flat plate $C_{df}\times10^3$	Riblet $C_{dr}\times10^3$	**Drag reduction (%)**
A	7.02	7.07	**-0.7**
B	8.23	7.63	**7.3**
C	8.22	7.65	**6.9**

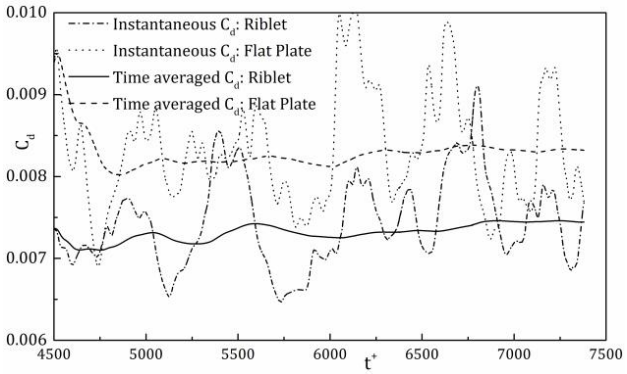

Fig. 3 Time history of drag coefficient at both flat and riblet walls for grid

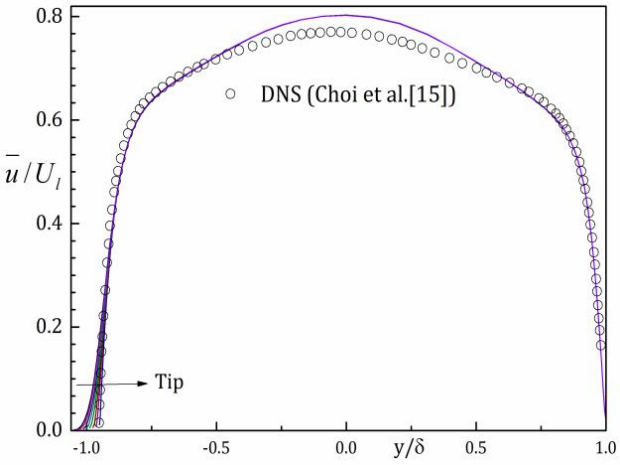

Fig. 4 Mean velocity profiles normalized by laminar velocity at different span wise locations

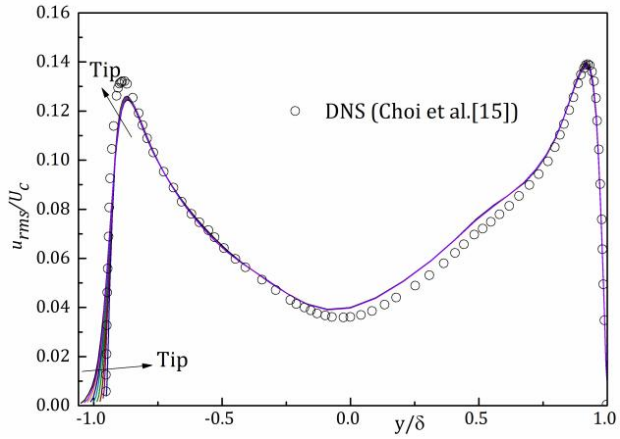

Fig. 5 Stream wise velocity fluctuations normalized by mean centerline velocity

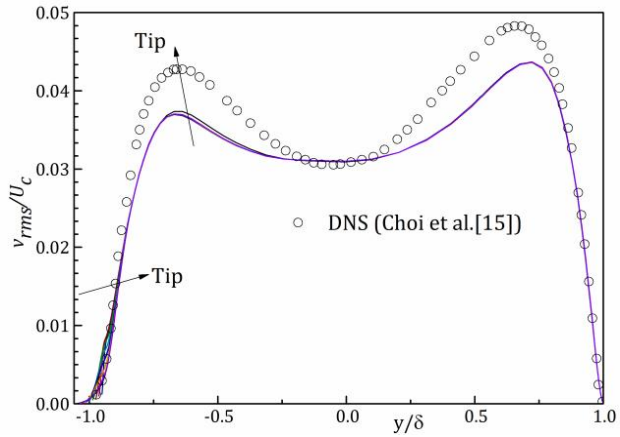

Fig. 6 Normal velocity fluctuations normalized by mean centerline velocity

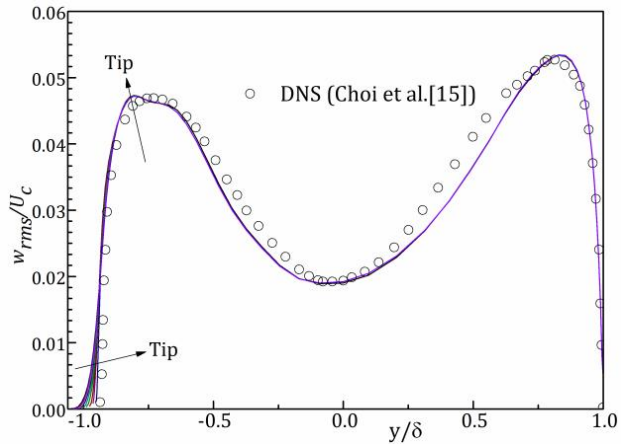

Fig. 7 Span wise velocity fluctuations normalized by mean centerline velocity

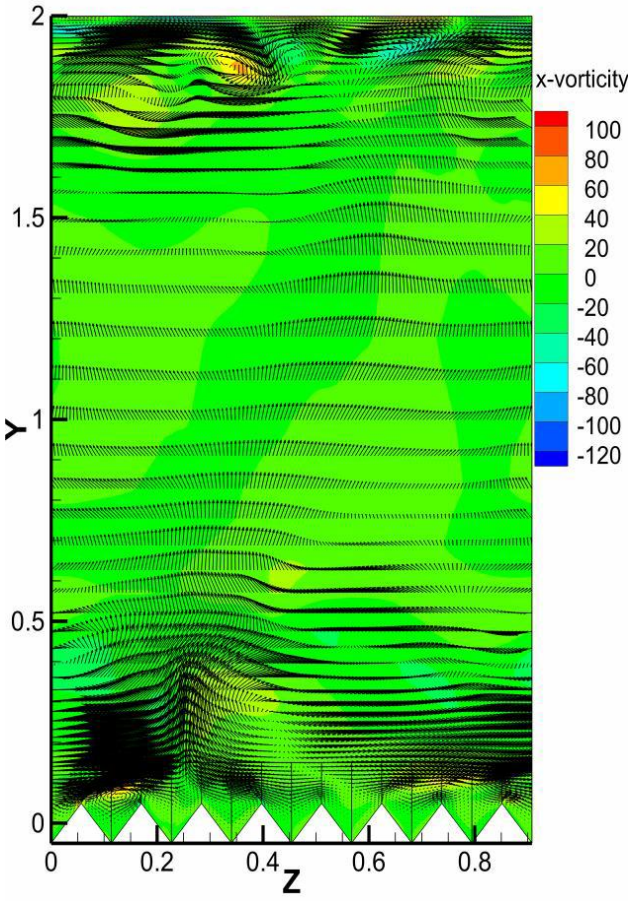

Fig. 8 Cross-flow velocity vectors (v,w) and contour of stream wise vorticity in y-z plane

Flow structures and drag reduction mechanism: It is known riblet surfaces exhibit drag reduction by impeding the translation of the streamwise vortices, which causes a reduction in vortex ejection and outer-layer turbulence. Also, riblets lift the vortices off the surface and reduce the amount of surface area exposed to the high-velocity flow [5].

The transverse-flow structures leading to drag reduction can be seen in the cross-sectional views as shown in Fig. 8. Fig. 8 shows cross-flow velocity vectors (v, w) embedded with the streamwise vorticity contours in the transverse plane. As it is shown, the strengths of the streamwise vortices above the riblets are reduced as compared to flat wall, suggesting that the downwash and ejection motions due to the streamwise vortices are weakened. Also, large secondary motion can be observed outward the riblets and there are no vortices in riblet valleys. These streamwise vortices stay above the riblets because their average diameter is larger than the spacing of the riblets.

It is observed in Fig. 8 that Cross-flow velocity in riblet valleys is low, confirming the idea of impeding of the streamwise vortices by riblets. These show a decrease of the momentum transport which results in Reynolds stresses reduction near the riblets.

IV. CONCLUSION

Large Eddy Simulations of turbulent flow over V-shaped riblet surfaces were performed at the friction Reynolds number . LES results were compared with DNS of Choi et al. [15] and good quantitative agreement was obtained for WALE SGS model, confirming that the LES method is capable of modeling the turbulent structure over riblet wall.

From this calculation study, it was shown that velocity flactuations over riblets were decreased compared to flat wall. More reduction of the normal and spanwise velocity fluctuations above the riblets indicated that the cross-flow is more sensitive to the presence of riblets than the flow in the streamwise direction. Also, cross-flow examination showed that most streamwise vortices are above riblet tips. Moreover, the strengths of those vortices above the riblets are reduced compared to flat wall. So, the tip region is exposed to high shear rate induced by them and most areas of the surface have low shear stress. This is the main reason of net drag reduction over riblet surfaces.

ACKNOWLEDGMENTS

The computations of this study are performed at the High Speed Computing Center in the department of Mechanical and aerospace Engineering of Shiraz University of Technology. Also, Support from the Marine Systems Research center is gratefully acknowledged.

REFERENCES

[1] Kodama, Y., Kakugawa, A., Takahashi, T. and Kawashima, H., "Experimental study on microbubbles and their applicability to ships for skin friction reduction", International Journal of Heat and Fluid Flow, Vol. 21, No. 5, 582-588, 2000.

[2] Truong, V.-T., "Drag reduction technologies", DSTO-GD-0290, DSTO Aeronautical and Maritime Research Laboratory, 2001.

[3] Gad-el-Hak, M., "Compliant coatings for drag reduction", Progress in Aerospace Sciences, Vol. 38, No. 1, 77-99, 2002.

[4] Bhushan, B. and Jung, Y.C., "Natural and biomimetic artificial surfaces for superhydrophobicity, self-cleaning, low adhesion, and drag reduction", Progress in Materials Science, Vol. 56, No. 1, 1-108, 2011.

[5] Dean, B. and Bhushan, B., "Shark-skin surfaces for fluid-drag reduction in turbulent flow: a review", Philosophical Transactions of the Royal Society A: Mathematical, Physical and Engineering Sciences, Vol. 368, No. 1929, 4775-4806, 2010.

[6] Walsh, M.J., "Drag Characteristics of V-Groove and Transverse Curvature Riblets", Viscous Flow Drag Reduction, American Institute of Aeronautics and Astronautics, 168-184, 1980.

[7] Walsh, M.J., "Turbulent boundary layer drag reduction using riblets", 20th Aerospace Sciences Meeting, Orlando, Florida, USA, January 11-14, 1982.

[8] Walsh, M.J., "Riblets as a Viscous Drag Reduction Technique", AIAA Journal, Vol. 21, No. 4, 485-486, 1983.

[9] Walsh, M.J., "Effect of detailed surface geometry on riblet drag reduction performance", Journal of Aircraft, Vol. 27, No. 6, 572-573, 1990.

[10] Bechert, D.W., Bruse, M., Hage, W., Van der hoeven, J.G.T. and Hoppe, G., "Experiments on drag-reducing surfaces and their optimization with an adjustable geometry", Journal of Fluid Mechanics, Vol. 338, 59-87, 1997.

[11] Bechert, D.W., Bruse, M. and Hage, W., "Experiments with three-dimensional riblets as an idealized model of shark skin", Experiments in Fluids, Vol. 28, No. 5, 403-412, 2000.

[12] Lee, S.J. and Lee, S.H., "Flow field analysis of a turbulent boundary layer over a riblet surface", Experiments in Fluids, Vol. 30, No. 2, 153-166, 2001.

[13] Goldstein, D., Handler, R. and Sirovich, L., "Direct numerical simulation of turbulent flow over a modelled riblet covered surface", Journal of Fluid Mechanics, Vol. 302, 333-376, 1995.

[14] El-Samni, O.A., Chun, H.H. and Yoon, H.S., "Drag reduction of turbulent flow over thin rectangular riblets", International Journal of Engineering Science, Vol. 45, No. 2–8, 436-454, 2007.

[15] Choi, H., Moin, P. and Kim, J., "Direct numerical simulation of turbulent flow over riblets", Journal of Fluid Mechanics, Vol. 255, 503-539, 1993.

[16] Launder, B.E. and Li, S.P., "On the prediction of riblet performance with engineering turbulence models", Applied Scientific Research, Vol. 50, No. 3-4, 283-298, 1993.

[17] Benhamza, M. and Belaid, F., "Computation of turbulent channel flow with variable spacing riblets", Mechanika, Vol. 5, No. 79, 36-41, 2009.

[18] Djenidi, L. and Antonia, R.A., "Riblet flow calculation with a low Reynolds number - ε model", Applied Scientific Research, Vol. 50, No. 3-4, 267-282, 1993.

[19] Peet, Y., Sagaut, P. and Charron, Y., "Towards Large Eddy Simulations of Turbulent Drag Reduction Using Sinusoidal Riblets", Proceedings of the 5th IASME / WSEAS International Conference on Fluid Mechanics and Aerodynamics, Athens, Greece, (August 25-27, 2007), 2007.

[20] Peet, Y., Sagaut, P. and Charron, Y., "Turbulent Drag Reduction Using Sinusoidal Riblets With Triangular Cross-Section", 38th Fluid Dynamics Conference and Exhibit, Seattle, USA, (June 23-26, 2008), 2008.

[21] Nicoud, F. and Ducros, F., "Subgrid-Scale Stress Modelling Based on the Square of the Velocity Gradient Tensor", Flow, Turbulence and Combustion, Vol. 62, No. 3, 183-200, 1999.

[22] Menter, F.R., "Two-equation eddy-viscosity turbulence models for engineering applications", AIAA Journal, Vol. 32, No. 8, 1598-1605, 1994.